Available online at www.sciencedirect.com
SCIENCE DIRECT®
ELSEVIER
European Journal of Mechanics B/Fluids 24 (2005) 448–456
EUROPEAN JOURNAL OF MECHANICS B/FLUIDS

Supersonic triple deck flow past an eroding hump

Tarek M.A. El-Mistikawy [a,*], Fayza M.N. El-Fayez [b]

[a] *Department of Engineering Mathematics and Physics, Faculty of Engineering, Cairo University, Giza 12211, Egypt*
[b] *Department of Mathematics, Girls College of Education, P.O. Box 27104, Riyadh 11417, Saudi Arabia*

Received 2 March 2004; received in revised form 11 May 2004; accepted 21 October 2004

Available online 15 December 2004

Abstract

The problem of laminar supersonic flow past an eroding hump is formulated on the basis of the triple deck theory. The resulting lower deck problem is intrinsically unsteady with a moving boundary, the hump surface. Numerical solutions are obtained, starting from a steady hump flow till the hump and its contamination particles are totally removed from the computational domain. Typical results are presented; showing how the erosion of the hump progresses, and how the contamination spreads. The effect of the Schmidt number is also studied. The results attest to the validity of the triple deck model as well as the numerical solution method.

Keywords: Supersonic triple deck; Moving boundary; Eroding hump; Contamination; Numerical solution

1. Introduction

Flows past surfaces that erode, contaminating the fluid, are encountered in many situations. An example of environmental impact is the contamination of air as wind passes over piles of chemical waste or sand hills. Another example is re-entry flights, which involve ablation of surface coating at supersonic speeds to guard against overheating. Erosion caused by fluid flow is also used for machining and polishing of surfaces.

To understand the erosion process and estimate the extent and time scale of the contamination process, we study the supersonic flow past a hump that erodes shedding its particles to the flow. The mathematical model we choose is that of the triple deck theory [1]. It is an asymptotic model valid in the limit of infinite Reynolds number that takes into account the strong viscid/inviscid interaction, which accompanies fast streamwise changes.

Numerous triple deck problems can be found in the literature. The one of concern to the present work is the flow past a hump. The steady two-dimensional problem was first formulated by Smith [2] and solved numerically by Napolitano, Davis and Werle [3]. Smith, Sykes and Brighton [4] handled a three-dimensional hump. Sykes [5] included upper deck stratification in his steady hump flow. The unsteady hump problem was analyzed by Duck [6,7] and Bodonyi et al. [8]. The unsteadiness is externally imposed on the flow, and interest is mainly directed toward wave formation.

* Corresponding author.
E-mail address: mistik@link.net (T.M.A. El-Mistikawy).

0997-7546/$ – see front matter
doi:10.1016/j.euromechflu.2004.10.005

Nomenclature

a^*	sonic speed
A	displacement function
c (C)	concentration (normalized)
c_s (C_s)	saturation concentration (normalized)
f^* (F)	height of hump (normalized)
G	concentration gradient function
h^*	enthalpy
i (I)	counter of X-grid lines (end value)
$\mathcal{I}$	identity tensor
j (J)	counter of y-grid lines (end value)
ℓ^*	length of hump
L^*	length of flat plate preceding hump
Ma	freestream Mach number
p^* (P)	pressure (normalized)
Q	pressure gradient function
r	relaxation factor
R^*	gas constant
Re	freestream Reynolds number
Sc	Schmidt number
t^* (T)	time (normalized)
$\mathfrak{F}^*$	shear stress tensor
u^* (U)	longitudinal velocity (normalized)
v^* (V, v)	lateral velocity (normalized, shifted)
$\mathbf{v}^*$	velocity vector
W	shear function
x^* (X)	longitudinal coordinate (normalized)
y^* (Y, y)	lateral coordinate (normalized, shifted)

Greek letters

β	Mach factor; $\beta = \lvert Ma^2 - 1\rvert^{1/2}$
γ, γ'	ratio of specific heats, $\gamma' = \gamma/(\gamma - 1)$
$\boldsymbol{\Gamma}^*$	body force per unit volume
δ	y-step size
Δ	X-step size
ε	small parameter; $\varepsilon = Re^{-1/8}$
η_A, η_{be}, η_F	convergence tolerances
θ^*	temperature
κ^*	heat conductivity
λ^*	diffusion coefficient
μ^* (μ'^*)	first (second) viscosity
π_z	normalization factor for z
ρ^*	density of fluid
σ^*	density of hump
τ	boundary layer shear stress
φ^*	surface function
ω	reciprocal of time step size

Operators

D^*	substantial derivative
$\boldsymbol{\nabla}^*$	gradient
$(\,),_z$	derivative of ( ) with respect to z

Subscripts

b (B)	current (initial) beginning point of hump
e (E)	current (initial) ending point of hump
o	initial
s	surface
∞	freestream

Superscripts

k	iteration counter
n	time level counter
$*$	dimensional quantity

The present problem has several new features that distinguish it from previously handled triple deck problems, and make its numerical solution a difficult task. It is unsteady; the unsteadiness being intrinsic due to the erosion process. The surface of the hump is a moving boundary that diminishes both longitudinally and laterally. The concentration enters as an additional variable, together with its transport equation and abruptly changing boundary conditions.

Nonetheless, it was possible to compute a solution, starting from a steady state hump flow till the complete removal of the hump and its contamination particles from the computational domain. The moving boundary of the hump was transformed into a fixed one through an unsteady version of Prandtl's transposition (shift) theorem [9]. The steady problem was solved by the efficient steady solver of El-Mistikawy [10]; which adopted a non-iterative, second order accurate streamwise marching technique. The solution of the unsteady problem advanced in time in an iterative implicit manner with first order accuracy. All terms in the problem were represented in the new time level; except for the time derivative terms, which used backward representation. The resulting problem, being as close as could be to the steady problem, was solved by the steady solver.

The numerical results give plausible account of the erosion and contamination processes. The effect of the Schmidt number *Sc*, representing the ratio of momentum to concentration diffusivities, is explored. As expected, an increase in *Sc* is found to cause a decrease in the erosion rate and lateral spread of the contaminant; in accordance with the limiting behavior as *Sc* grows indefinitely.

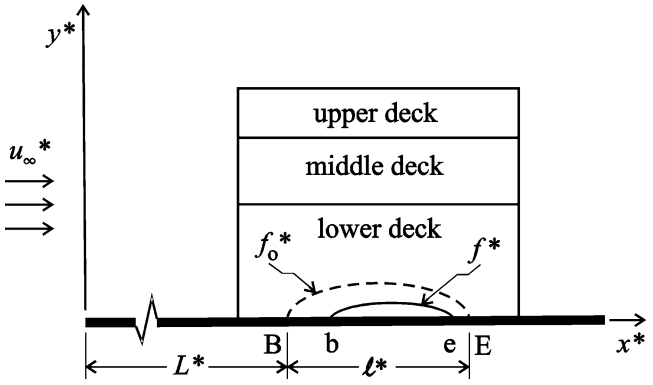

Fig. 1. Flow configuration.

2. Statement of the problem

A two-dimensional laminar compressible flow along a semi-infinite flat plate encounters a contamination spot in the form of a hump (Fig. 1). At the leading edge of the plate, we introduce Cartesian coordinate axes: x^* along the plate pointing downstream and y^* in the outward lateral direction. The hump has density σ^*. It begins at point B at a distance L^* from the leading edge, and extends a distance ℓ^* to end at point E. Its height is described by

$$y^* = f_0^*(x^* - L^*), \qquad L^* \leqslant x^* \leqslant L^* + \ell^*. \tag{1a}$$

The whole surface is maintained at a fixed temperature θ_s^* at which the clean fluid has density ρ_s^* and viscosity μ_s^*, and admits saturation concentration c_s and diffusion coefficient λ_s^*.

Far from the surface, the uncontaminated freestream has uniform velocity u_∞^* in the x^* direction, temperature θ_∞^*, density ρ_∞^*, pressure p_∞^*, sonic speed a_∞^*, and viscosity μ_∞^*. The freestream is supersonic with Mach number $Ma = u_\infty^*/a_\infty^* > 1$. The Reynolds number $Re = \rho_\infty^* u_\infty^* L^*/\mu_\infty^*$ is large and relates to a diminishing parameter $\varepsilon = Re^{-1/8}$.

For $\ell^* = \mathrm{O}(\varepsilon^3 L^*)$ and $f_0^* = \mathrm{O}(\varepsilon^5 L^*)$, the boundary layer structure forming upstream of the hump develops into a triple deck structure around the hump. The lower deck problem for this steady flow was obtained by Smith [2] and solved numerically by Napolitano et al. [3].

At time $t^* = 0$, erosion starts as particles of the hump diffuse into the flow to be washed downstream by the oncoming clean fluid. The contamination is, therefore, confined to the lower deck and its downstream continuation. The steady triple deck structure remains intact; however, the lower deck has to be corrected for the unsteady contamination process. The lower deck variables show dependence on the time t^*, which has to be $\mathrm{O}(\varepsilon^2 L^*/u_\infty^*)$ for the unsteadiness to be of leading order effect. In particular, the hump is, now, described by

$$y^* = f^*(x^* - L^*, t^*), \qquad x_b^*(t^*) \leqslant x^* \leqslant x_e^*(t^*), \tag{1b}$$

where $f^*(x^* - L^*, 0) = f_0^*(x^* - L^*)$, $x_b^*(0) = x_B^* = L^*$, and $x_e^*(0) = x_E^* = L^* + \ell^*$.

(Henceforth, f^* is extended to describe the entire surface, given zero value outside the interval $x_b^* < x^* < x_e^*$. The entire surface can therefore be described by $y^* = f^*$, or alternatively, by $\varphi^*(x^*, y^*, t^*) = 0$ where $\varphi^* = y^* - f^*$.)

The governing continuity, momentum, concentration, and energy equations are written here for completeness. For details, see, for example, reference [11].

$$D^*\rho^* + \rho^* \nabla^* \cdot \mathbf{v}^* = 0, \tag{2a}$$

$$\rho^* D^* \mathbf{v}^* + \nabla^* p^* = \nabla^* \cdot \mathfrak{F}^* + \boldsymbol{\Gamma}^*, \tag{2b}$$

$$\rho^* D^* c = \nabla^* \cdot (\lambda^* \nabla^* c), \tag{2c}$$

$$\rho^* D^* h^* - D^* p^* = \mathfrak{F}^* : \nabla^* \mathbf{v}^* + \nabla^* \cdot (\kappa^* \nabla^* \theta^*). \tag{2d}$$

They are supplemented by the perfect gas laws

$$p^* = R^* \rho^* \theta^*, \quad a^{*2} = \gamma R^* \theta^*, \quad h^* = \gamma' R^* \theta^* \tag{2e–g}$$

and the constitutive relation for the shear stress tensor $\mathfrak{F}^*$

$$\mathfrak{F}^* = \mu^* \left[\nabla^* \mathbf{v}^* + (\nabla^* \mathbf{v}^*)^{\#} \right] + \mu'^* (\nabla^* \cdot \mathbf{v}^*) \boldsymbol{\mathcal{I}}. \tag{2h}$$

Respectively, D^* and $\boldsymbol{\nabla}^*$ are the operators of substantial derivative and gradient. ρ^*, p^*, θ^*, h^*, a^*, c, and $\mathbf{v}^* = (u^*, v^*)$ are the density, pressure, temperature, enthalpy, sonic speed, concentration, and velocity vector. λ^*, κ^*, μ^*, and μ'^* are the coefficients of diffusion, heat conductivity, first viscosity, and second viscosity. R^* is the gas constant. γ is the ratio of specific heats and $\gamma' = \gamma/(\gamma - 1)$. $\boldsymbol{\mathcal{I}}$ is the identity tensor, and $(\boldsymbol{\nabla}^*\mathbf{v}^*)^{\#}$ is the transpose of $\boldsymbol{\nabla}^*\mathbf{v}^*$. $\boldsymbol{\Gamma}^*$ is the body force per unit volume.

The conditions at the surface are, concisely,

$$\mathbf{v}^* \times \boldsymbol{\nabla}^*\varphi^* = 0, \quad D^*\varphi^* = 0, \quad \lambda^*\boldsymbol{\nabla}^* c \cdot \boldsymbol{\nabla}^*\varphi^* = \sigma^*\mathbf{v}^* \cdot \boldsymbol{\nabla}^*\varphi^*. \tag{3a–c}$$

The first is the no-slip condition, forcing the velocity vector to be along the normal to the hump surface $\boldsymbol{\nabla}^*\varphi^*$. The second is the adherence condition, insuring that the fluid element adjacent to the hump surface follows the surface in its motion. The third is the Stefan condition, equating the rate at which the contaminant diffuses into the fluid to the rate at which the contamination particles are removed from the hump. In addition, the saturation condition

$$c = c_{\mathrm{s}} \tag{3d}$$

applies at the hump surface.

Carrying out the usual triple deck analysis (taking the Schmidt number $Sc = \mu_{\mathrm{s}}^*/\lambda_{\mathrm{s}}^*$ to be O(1) and neglecting the body force term) leads to a lower deck problem that can be written as follows (a comma followed by a subscript denotes differentiation).

$$U_{,X} + V_{,Y} = 0, \tag{4a}$$

$$U_{,T} + UU_{,X} + U_{,Y}V + P_{,X} = U_{,YY}, \quad P_{,Y} = 0, \tag{4b,c}$$

$$C_{,T} + UC_{,X} + C_{,Y}V = Sc^{-1}C_{,YY}, \tag{4d}$$

$$U = 0, \quad V = F_{,T} = Sc^{-1}C_{,Y}, \quad C = C_{\mathrm{s}} \quad \text{at } Y = F(X,T),\ X \in \big[X_{\mathrm{b}}(T),\ X_{\mathrm{e}}(T)\big], \tag{4e–h}$$

$$U = 0, \quad V = 0 = C_{,Y} \quad \text{at } Y = 0,\ X \notin \big[X_{\mathrm{b}}(T), X_{\mathrm{e}}(T)\big], \tag{4i–k}$$

$$U_{,Y} \sim 1, \quad U \sim Y - A(X,T), \quad C \sim 0 \quad \text{as } Y \sim \infty, \tag{4l–n}$$

$$U \sim Y, \quad A \sim 0, \quad C \sim 0 \quad \text{as } X \sim -\infty, \tag{4o–q}$$

$$P \sim 0 \quad \text{as } X \sim \infty, \tag{4r}$$

$$P = A_{,X}. \tag{4s}$$

All lower deck variables are normalized. The Cartesian coordinates (X, Y), hump height F, velocity components (U, V), concentration C, pressure P, and time T are related to the corresponding physical variables x^*, y^*, f^*, u^*, v^*, c, p^*, and t^* as follows:

$$x^* - L^* = \varepsilon^3\pi_x X L^*, \quad y^* = \varepsilon^5\pi_y Y L^*, \quad f^* = \varepsilon^5\pi_y F L^*, \tag{5a–c}$$

$$u^* = \varepsilon\pi_u U u_\infty^*, \quad v^* = \varepsilon^3\pi_v V u_\infty^*, \quad c = \pi_c C, \tag{5d–f}$$

$$p^* - p_\infty^* = \varepsilon^2\pi_p P\rho_\infty^* u_\infty^{*2}, \quad t^* = \varepsilon^2\pi_t T L^*/u_\infty^*. \tag{5g,h}$$

The π's are normalization factors given by

$$\pi_x = \rho_{\mathrm{s}}^{-1/2}\mu_{\mathrm{s}}^{-1/4}\beta^{-3/4}\tau^{-5/4}, \quad \pi_y = \rho_{\mathrm{s}}^{-1/2}\mu_{\mathrm{s}}^{1/4}\beta^{-1/4}\tau^{-3/4}, \tag{6a,b}$$

$$\pi_u = \rho_{\mathrm{s}}^{-1/2}\mu_{\mathrm{s}}^{1/4}\beta^{-1/4}\tau^{1/4}, \quad \pi_v = \rho_{\mathrm{s}}^{-1/2}\mu_{\mathrm{s}}^{3/4}\beta^{1/4}\tau^{3/4}, \tag{6c,d}$$

$$\pi_c = \sigma^*/\rho_{\mathrm{s}}^*, \quad \pi_p = \mu_{\mathrm{s}}^{1/2}\beta^{-1/2}\tau^{1/2}, \quad \pi_t = \mu_{\mathrm{s}}^{-1/2}\beta^{-1/2}\tau^{-3/2}, \tag{6e–f}$$

where $\rho_{\mathrm{s}} = \rho_{\mathrm{s}}^*/\rho_\infty^*$ and $\mu_{\mathrm{s}} = \mu_{\mathrm{s}}^*/\mu_\infty^*$; $\beta = |Ma^2 - 1|^{1/2}$ is the Mach factor; while τ is a non-dimensional constant representing the surface shear of the clean boundary layer, as it approaches the hump region.

Conditions (4e–g) are normalized leading order forms of the no-slip, adherence, and Stefan conditions (3a–c). So are conditions (4i–k) but for $f^* = 0$ (i.e. $\varphi^* = y^*$). The saturation condition (4h) completes the conditions at the hump surface.

Conditions (4l–n), (4o–q), and (4r) are matching conditions to the middle deck, the lower part of the oncoming boundary layer, and the downstream continuation of the lower deck, respectively. In particular, conditions (4n) and (4q) indicate that the flow in the middle deck and the oncoming flow are uncontaminated.

Finally, the interaction law (4s) expresses the sustained interaction between the supersonic potential flow in the upper deck and the viscous flow in the lower deck. It relates the pressure perturbation produced in the former to the displacement effect produced in the latter; A being an unknown displacement function defined by condition (4m).

The initial conditions at $T = 0$ for the unsteady problem (4) result as the solution of the steady problem; which can be obtained by dropping all time derivative terms together with the saturation condition (4h), and setting $F(X, 0) = F_{\mathrm{o}}(X)$, $X_{\mathrm{b}}(0) = X_{\mathrm{B}} = 0$ and $X_{\mathrm{e}}(0) = X_{\mathrm{E}}$. The concentration equation (4d) and its boundary conditions (4k), (4n), and (4q), then, have the solution of everywhere clean initial flow $C = 0$.

3. Numerical solution

The lower deck problem (4) has a moving boundary that diminishes in size, both longitudinally and laterally, causing intrinsic unsteadiness that is not externally imposed on the flow. The hump height $F(X,T)$ as well as its nonzero interval $X_b(T) < X < X_e(T)$ has to be determined as a part of the solution.

3.1. Reformulation

It proved beneficial, in handling the steady problem (e.g. [2] and [3]), to apply Prandtl's shift [9]

$$y = Y - F_o, \qquad v = V - U F_{o,X} \tag{7a,b}$$

in order to transfer the surface conditions to the line $y = 0$. Likewise, for the unsteady problem, we apply the unsteady shift

$$y = Y - F, \qquad v = V - U F_{,X} - F_{,T}. \tag{8a,b}$$

Note that v in the steady problem and the initial value (at $T = 0$) of v in the unsteady problem are not the same. They differ by $F_{,T}(X,0)$, as the shift rules (7b) and (8b) for v indicate. Moreover, the shift results in discontinuities in v across the lines $X = X_b$ and $X = X_e$ due to the discontinuity in $F_{,X}$.

We next introduce the shear function $W(X,y,T)$, the concentration gradient function $G(X,y,T)$, and the pressure gradient function $Q(X,T)$, as defined below in Eqs. (9c), (9e), and (9u), in order to recast problem (4) in the new form

$$U_{,X} + v_{,y} = 0, \tag{9a}$$

$$U_{,T} + UU_{,X} + U_{,y}v + Q = W_{,y}, \quad W = U_{,y}, \tag{9b,c}$$

$$C_{,T} + UC_{,X} + C_{,y}v = Sc^{-1}G_{,y}, \quad G = C_{,y}, \tag{9d,e}$$

$$U = 0, \quad v = 0, \quad F_{,T} = Sc^{-1}G, \quad C = C_s \quad \text{at } y = 0,\ X \in [X_b, X_e], \tag{9f–i}$$

$$U = 0, \quad v = 0, \quad G = 0 \quad \text{at } y = 0,\ X \notin [X_b, X_e], \tag{9j–l}$$

$$W \sim 1, \quad U \sim y - A + F, \quad C \sim 0 \quad \text{as } y \sim \infty, \tag{9m–o}$$

$$U \sim y, \quad A \sim 0, \quad C \sim 0 \quad \text{as } X \sim -\infty, \tag{9p–r}$$

$$P \sim 0 \quad \text{as } X \sim \infty, \tag{9s}$$

$$P = A_{,X}, \quad Q = P_{,X}. \tag{9t,u}$$

It is noted that the concentration field affects the velocity field only through varying the surface height as expressed by condition (9h).

3.2. Time discretization

Contrary to the popular practice of modeling a steady solver after an unsteady one, the present work relies on modeling an unsteady solver after a successful steady one. All terms in problem (9) are expressed in the new time level $n+1$, except for the time derivative terms which are expressed with first order accuracy using the backward difference representations $U_{,T} = \omega^n(U^{n+1} - U^n)$, $C_{,T} = \omega^n(C^{n+1} - C^n)$, and $F_{,T} = \omega^n(F^{n+1} - F^n)$ where $\omega^n = (T^{n+1} - T^n)^{-1}$. The resulting problem is as close as possible to the steady problem and is, therefore, solved by a steady solver. All we need from the old time level n is U^n, C^n, and F^n. This reduces the storage requirements and avoids having to use v^n, which is discontinuous at the initial time level $n = 0$.

3.3. Iterative procedure

The steady solver we choose is El-Mistikawy's method [10]. It is an efficient iterative method that takes, in the kth iteration, an old distribution A^k of the displacement function and produces a new one A^{k+1}. All equations and conditions in problem (9) are expressed in the new iteration level $k+1$, except for condition (9m) which is written as follows

$$U^{k+1} \sim y - A^k + F^k \quad \text{as } y \sim \infty \tag{9m′}$$

and Eq. (9u) which is replaced by the relaxation relation

$$P^{k+1}{}_{,X} - Q^{k+1} = r(A^{k+1} - A^k), \tag{9u′}$$

where r is a relaxation factor. That F is given its old value F^k in condition (9m′) is in accord with F being fixed (i.e. known) in the steady problem. (For convenience, the superscripts $n+1$ and $k+1$ will be dropped, henceforth.)

3.4. Computational domain and layout

The computational domain covers the region of the Xy-plane described by $X_{-\infty} \leqslant X \leqslant X_{+\infty}$, $0 \leqslant y \leqslant y_{+\infty}$, where $-X_{-\infty}$, $X_{+\infty}$ and $y_{+\infty}$ are large enough to allow for adequate enforcement of the asymptotic conditions (9m–s). It is divided into rectangular cells by a grid of (i)-lines $X = X(i)$ and (j)-lines $y = y(j)$. The counter $i = 1 \to I$ is such that $X(1) = X_{-\infty}$, $X(i_B) = X_B$, $X(i_b) = X_b$, $X(i_e) = X_e$, $X(i_E) = X_E$, and $X(I) = X_{+\infty}$; while the counter $j = 1 \to J$ is such that $y(1) = 0$ and $y(J) = y_{+\infty}$. The typical ij-cell has X-step $\Delta(i) = X(i) - X(i-1)$ and y-step $\delta(j) = y(j) - y(j-1)$, and through its midpoint pass the $(i - \frac{1}{2})$ and $(j - \frac{1}{2})$-lines.

El-Mistikawy's method [10], as applied to the steady problem, involves implicit marching in the X-direction that advances the solution non-iteratively from an i-line to the next, and uses three-point representation in the X-direction to achieve second order accuracy. Its success can be attributed to the discretization layout it adopts; namely, U is assigned to the grid points (i, j) whereas v and W are assigned to the points $(i - \frac{1}{2}, j)$. For the unsteady problem, comparison of Eqs. (9b,c) to Eqs. (9d,e) shows that C and G play the roles of U and W, respectively. They are, therefore, assigned to the same points; C to (i, j) and G to $(i - \frac{1}{2}, j)$. Moreover, similar finite difference representations are applied to similar terms in the compared equations. The X-dependent variables A and P are assigned to the i-lines, whereas Q is assigned to the $(i - \frac{1}{2})$-lines. As for the hump height, F is assigned to the i and $(i - \frac{1}{2})$-lines.

3.5. Space discretization

Eqs. (9a–e) are centered at the midpoint of the ij-cell. Central difference expressions, in terms of the abovementioned layout, are used throughout. However, U the coefficient of $U_{,X}$ and $C_{,X}$ in Eqs. (9b,d) and $U_{,y}$ in Eqs. (9b,c) are represented in terms of the $(i - \frac{1}{2})$-values of U, then $U(i - \frac{1}{2}, j)$ is expressed backwards as $U(i-1, j) + \frac{1}{2}\Delta(i)U_{,X}(i - \frac{1}{2}, j)$ in Eqs. (9b,d) and forwards as $U(i, j) - \frac{1}{2}\Delta(i)U_{,X}(i - \frac{1}{2}, j)$ in Eq. (9c). For these representations to be second order accurate in the X-direction, $U_{,X}(i - \frac{1}{2}, j)$ may be represented with first order accuracy. At $i = 2$, we set $U_{,X}(i - \frac{1}{2}, j) = 0$ in accordance with condition (9p). Next to the two lines $i = i_b$ and $i = i_e$ where v (and consequently $U_{,X}$) is discontinuous, we use the respective kth iterate $U^k{}_{,X}(i + \frac{3}{2}, j)$ with the representation $[U^k(i+2, j) - U^k(i+1, j)]/\Delta(i+2)$ to approximate $U_{,X}(i + \frac{1}{2}, j)$ and to represent $U_{,X}(i + \frac{3}{2}, j)$. Otherwise, since continuity permits, $U_{,X}(i - \frac{1}{2}, j)$ is approximated by its counterpart at the $(i - \frac{3}{2})$-line with the representation $[U(i-1, j) - U(i-2, j)]/\Delta(i-1)$. A treatment similar to that of $U_{,y}$ in Eqs. (9b,c) is applied to $C_{,y}$ in the corresponding Eqs. (9d,e).

At each i-line, the resulting $5(J-1)$ finite difference equations involve the $5J+1$ unknowns: $U(i, j)$, $C(i, j)$, $v(i - \frac{1}{2}, j)$, $W(i - \frac{1}{2}, j)$, and $G(i - \frac{1}{2}, j)$ for $j = 1 \to J$; together with $Q(i - \frac{1}{2})$. They are to be supplemented, in view of conditions (9f–o), with $U(i, 1) = 0$, $v(i - \frac{1}{2}, 1) = 0$, $C(i, 1) = C_s$ when $i_b < i \leqslant i_e$, $G(i - \frac{1}{2}, 1) = 0$ when $i \leqslant i_b$ or $i > i_e$, $W(i - \frac{1}{2}, J) = 1$, $U(i, J) = y_{+\infty} - A^k(i) + F^k(i)$, and $C(i, J) = 0$. This set of linear equations is efficiently solved for the unknowns by the appending (non-bordering) technique of reference [12].

3.6. Solution steps

At each new time level $n+1$, a two-step iterative procedure is performed. The first step of the kth iteration solves for U, v, C, W, G, and Q by marching in the X-direction, which starts at $i = 2$ (where conditions (9p,r) supply the needed values at $i = 1$) and ends at $i = I$. This is followed by evaluating a new distribution for F as follows. Condition (9h), expressed at the $(i - \frac{1}{2})$-lines, gives $F(i - \frac{1}{2}) = F^n(i - \frac{1}{2}) + Sc^{-1}G(i - \frac{1}{2}, 1)/\omega^n$ which is used to determine $F(i - \frac{1}{2})$, for $i_b < i \leqslant i_e$. The resulting $i_e - i_b - 1$ values together with the end conditions $F(i_b) = F(i_e) = 0$ suffice to determine $F(i)$ for $i_b < i < i_e$, when F is represented by quadratic splines so that F and $F_{,X}$ are continuous at each i-line.

In the second step of the kth iteration, we solve for P and A. Eqs. (9t) and (9u′) are centered at the $(i - \frac{1}{2})$-lines and central difference representations are used to achieve second order accuracy. Conditions (9q) and (9s) complete the set of equations which are solved to give $P(i)$ and $A(i)$ for $i = 1 \to I$.

Of the kth iterates only $F^k(i)$, $A^k(i)$, $U^k{}_{,X}(i_b + \frac{3}{2}, j)$, $U^k{}_{,X}(i_e + \frac{3}{2}, j)$, $C^k{}_{,X}(i_b + \frac{3}{2}, j)$, and $C^k{}_{,X}(i_e + \frac{3}{2}, j)$ need to be stored for use in the next iteration. Their first iterates (when $k = 1$) are taken from the solution at time level n.

The iterative process continues until A and F reach convergence as judged by the satisfaction, everywhere, of the inequalities $|A^{k+1}(i) - A^k(i)| < \eta_A$ and $|F^{k+1}(i) - F^k(i)| < \eta_F$ where η_A and η_F are prescribed tolerances. This marks the end of the present time step.

We advance in time, step by step. At the instant when either $F(i_b + 1)$ or $F(i_e - 1)$ becomes less than a prescribed tolerance η_{be}, we increase i_b by 1 or decrease i_e by 1, respectively, and set $F = 0$ there.

The steady problem is obtained by canceling the time derivative terms, dropping condition (9i), and setting $F^k = F_o$, $X_b = X_B$, and $X_e = X_E$ to describe the hump in its prescribed initial state. Its solution procedure is equivalent to one time step of the unsteady solver. It ends when A reaches convergence, starting from its guessed distribution $A = F_o$.

3.7. Implementation

We applied the numerical method explained above to a hump described by $F_o = 4X(1 - X)$; thus having $X_E = 1$. The computational domain extended to $X_{-\infty} = -10$, $X_{+\infty} = 16$, and $y_{+\infty} = 12$. The grid was such that $I = 131$, $J = 39$, $i_B = 36$, and $i_E = 61$. Variable step sizes in both directions were utilized to suit regions of fast or slow changes. Initially, the X-step size Δ took the values: 0.4 (for $1 < i \leqslant 6$ and $116 < i \leqslant 131$), 0.3 (for $6 < i \leqslant 26$ and $96 < i \leqslant 116$), 0.2 (for $26 < i \leqslant 36$ and $86 < i \leqslant 96$), 0.04 (for $36 < i \leqslant 61$ and $72 < i \leqslant 76$), 0.05 (for $76 < i \leqslant 80$), and 0.1 (for $80 < i \leqslant 86$). This left a gap of size 0.04 that followed $i = i_E$. It was divided by 10 i-lines into much smaller 11 steps; 5 of size 0.002, 3 of size 0.004, then 3 of size 0.006. As time passed, the end of the hump retracted, by steps of size 0.04, from $i = i_E$ to $i = i_e$. After each retraction, those 11 steps were transferred so that they always followed the new i_e-line. To put this transfer into effect, we only needed to perform a linear interpolation in order to produce $A(i)$ at the 10 i-lines $i_e < i < i_e + 11$ in their new location. The y-step size δ took the values: 0.02, 0.04, 0.06, and 0.08 each for one step, 0.1 for 2 steps, 0.2 for 6 steps, 0.3 for 8 steps, 0.4 for 10 steps, then 0.5 for the last 8 steps. For convergence tolerances, we chose $\eta_A = \eta_F = \eta_{be} = 10^{-4}$. A time step of size 0.2 was consistently used, unless a change in i_b or i_e was anticipated. Then, the instant of change was captured in one or two steps within a time interval of 0.4 involving three steps; each not exceeding 0.2. The suitable value for the relaxation factor r was 0.5 for the steady problem and 10 for the unsteady problem. These choices made it possible to proceed with the solution till a hump characterized by saturation concentration $C_s = 0.01$ was totally erased, and the contaminant was completely washed out of the computational domain. To study the effect of the Schmidt number, four values of Sc (0.2, 0.5, 1, and 2) were used.

4. Results

The results of the typical case ($Sc = 1$) agree with what one expects. The erosion in the front of the hump is faster than in its back. The originally symmetric hump progressively looses its symmetry. This is obvious in Fig. 2 showing the hump shape at different times of interval 20.

The contamination spreads laterally mainly by diffusion and longitudinally downstream mainly by convection. The contamination boundary, defined to be having concentration of 1% C_s, is shown in its development stage in Fig. 3(a) and afterwards in Fig. 3(b). It expands laterally then approaches a ceiling (at $T \approx 10$), as the oncoming clean fluid carries the contaminant further and further downstream till it reaches the computational boundary ($X = 16$). With the diminishment of the hump the ceiling falls gradually, and after the hump is completely removed (at $T \approx 106$) the contamination boundary travels downstream until it departs the computational domain (at $T \approx 118$). Fig. 4 presents several concentration contours at the instant $T \approx 16$ when

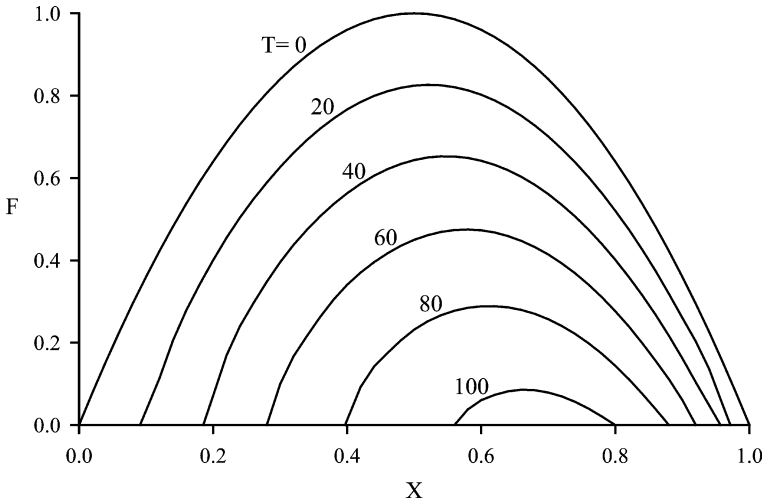

Fig. 2. Erosion of hump.

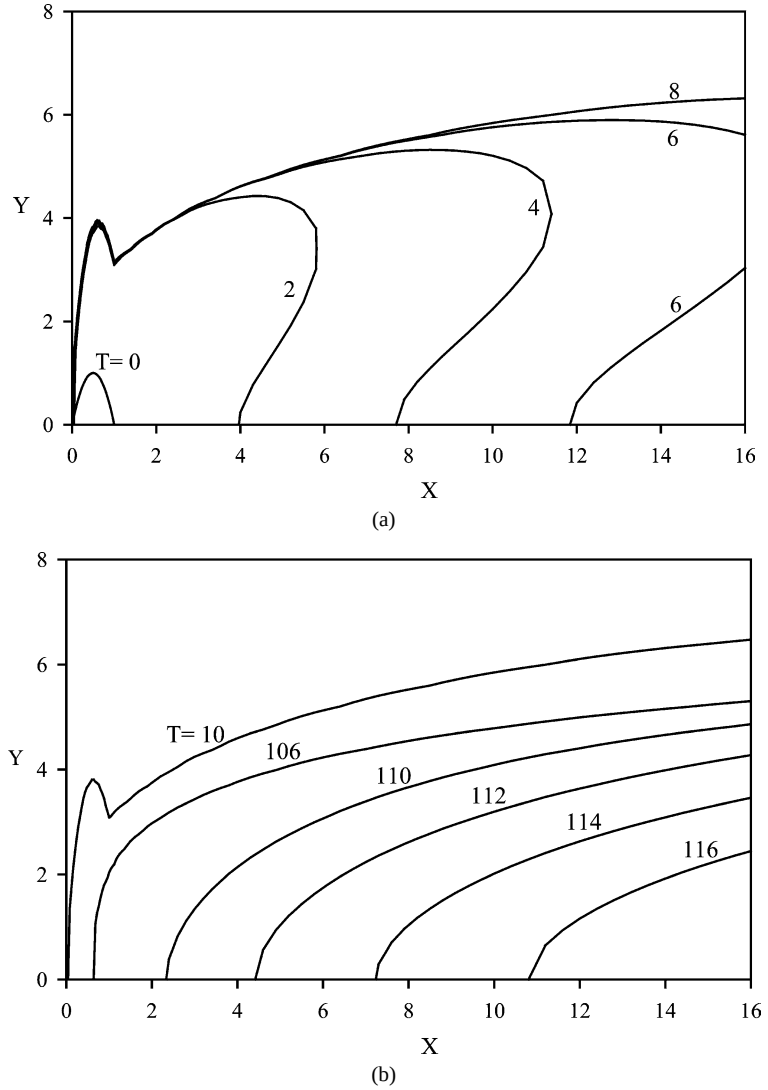

Fig. 3. Contamination boundary ($C/C_s = 1\%$). (a) early stages $0 \leqslant T \leqslant 8$; (b) later stages $T \geqslant 10$.

the 10% C_s contour reaches its farthest downstream extent. Higher concentration contours, likewise, extend to their farthest but earlier (e.g. at $T \approx 9$ for the 20% C_s contour); then retract slowly marking a slight prominence of convection over diffusion.

As expected, increasing the Schmidt number Sc leads to a decrease in the lateral extent of the contamination as well as in the erosion rate of the hump. The contamination ceiling at $X = 10$, for example, reaches $y \approx 9.90$, 7.34, 5.85, or 4.66 when $Sc = 0.2$, 0.5, 1, or 2, respectively. The corresponding time required for complete removal of the hump is $T \approx 37.1$, 67.4, 106.1, or 167.3. These trends are expected to persist as Sc increases indefinitely, since Eq. (9c) implies that a "concentration boundary layer" forms with $U \sim y \sim Sc^{-1/3}$ and $v \sim y^2 \sim Sc^{-2/3}$. Then, the rate of erosion $F_{,T}$ is found from condition (9h) to diminish as $Sc^{-2/3}$. This limiting behavior predicts a contamination ceiling that reaches $y \approx 10.00$, 7.37, 5.85, or 4.64 at $X = 10$ and a removal time $T \approx 36.3$, 66.8, 106.1, or 168.4, when proportionality to the case $Sc = 1$ is invoked; in remarkable agreement with the aforementioned numerical results.

5. Conclusion

In this paper, we have studied what we believe to be the first moving-boundary problem formulated within the framework of the triple deck theory. The supersonic flow past a flat surface having a contamination spot – in the form of a hump that erodes,

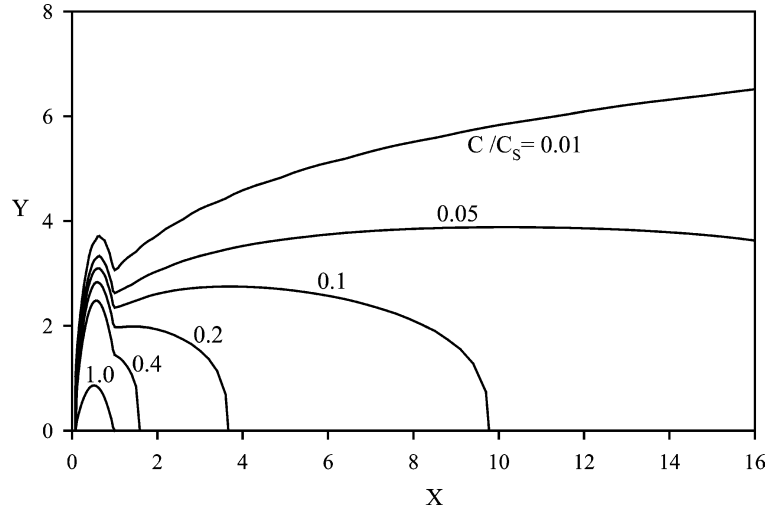

Fig. 4. Concentration contours at $T \approx 16$.

contaminating the flow – has been considered. The shape of the hump, which diminishes in size both longitudinally and laterally, needs to be determined as a part of the numerical solution process. The difficulties, associated with the erosion of the hump and the contamination of the flow, have been handled efficiently. The results indicate that the lateral spread of the contaminant is confined to a neighborhood of the surface that diminishes forming a concentration boundary layer, as the Schmidt number increases. Agreement with the scaling laws of this boundary layer is observed even for considerably law values of the Schmidt number.

References

[1] K. Stewartson, P.G. Williams, Self-induced separation, Proc. Roy. Soc. London Ser. A 312 (1969) 181–206.
[2] F.T. Smith, Laminar flow over a small hump on a flat plate, J. Fluid Mech. 57 (1973) 803–829.
[3] M. Napolitano, R.T. Davis, M.J. Werle, A numerical technique for the triple-deck problem, AIAA Paper, Number 78-1133, 1978.
[4] F.T. Smith, R.I. Sykes, P.W.M. Brighton, A two-dimensional boundary layer encountering a three-dimensional hump, J. Fluid Mech. 83 (1977) 163–176.
[5] R.I. Sykes, Stratification effects in boundary layer flow over hills, Proc. Roy. Soc. London Ser. A 361 (1978) 225–243.
[6] P.W. Duck, Laminar flow over a small unsteady hump on a flat plate, Mathematika 25 (1978) 24–35.
[7] P.W. Duck, Laminar flow over unsteady humps: the formation of waves, J. Fluid Mech. 160 (1985) 465–498.
[8] R.J. Bodonyi, W.J.C. Welch, P.W. Duck, M. Tadjfar, A numerical study of the interaction between unsteady free-stream disturbances and localized variations in surface geometry, J. Fluid Mech. 209 (1989) 285–308.
[9] C.W. Jones, E.J. Watson, Two-dimensional boundary layers, in: L. Rosenhead (Ed.), Laminar Boundary Layers, Oxford University Press, Oxford, 1966, pp. 211–212.
[10] T.M.A. El-Mistikawy, Separation prevention as an indirect problem based on the triple-deck theory, AIAA J. 32 (1994) 1423–1427.
[11] R.S. Brodkey, The Phenomena of Fluid Motions, Addison-Wesley, London, 1967.
[12] T.M.A. El-Mistikawy, Efficient solution of Keller's box equations for direct and inverse boundary layer equations, AIAA J. 32 (1994) 1538–1541.